Strain Analysis of Ridges on Europa

Sophia Zipparo

Date: 04/26/22

Advisors: Dr. Laurent Montési, Dr. Samuel Howell (JPL), and Karla Núñez

GEOL 394

Abstract:

Jupiter's icy moon Europa is a prime candidate in the search for the evolution of extraterrestrial life in our solar system. This is evidenced by the fact that Europa has a global subsurface ocean, which may have the necessary conditions to support life, beneath an icy shell. The study of ridges, global-scale linear features on the surface of Europa's ice shell, may give insights to if there may be transport of water between this global subsurface ocean and the surface of the ice shell. This study seeks to use the geometries associated with ridges and nearby background features to constrain the types and magnitudes of strain associated with ridge formation, which can in turn help to constrain the plausible formation mechanisms. Our results have shown small amounts of shear and normal strain associated with ridge formation. This implies that overprinting may be a dominant process in ridge formation.

Introduction and Background:

Europa is Jupiter's fourth largest moon. It is thought to have a rocky, silicate core with an outer ice shell and subsurface saltwater ocean (Anderson et al., 1998). Its ice shell may have a ductile lower asthenosphere and a brittle upper lithosphere (Howell & Pappalardo, 2018). The exact thickness of the ice shell is unknown, but estimates range from 3 to 40 km (Howell & Pappalardo, 2020). This structure can be seen in Figure 1. The surface of the ice shell is covered in geological features of varying morphologies, shown in Figure 2. The paucity of impact craters (Howell & Pappalardo, 2018) indicates a young surface age, which means that there has been resurfacing in Europa's recent geologic past. This relatively recent resurfacing may be related to the varying linear surface features. The presence of an induced magnetic field indicates that there is a liquid saltwater ocean (Khurana et al., 1998). There may be transport of water from the ocean to the surface, evidenced by the detection of water vapor plumes by the Hubble Space Telescope (Roth et al., 2014).

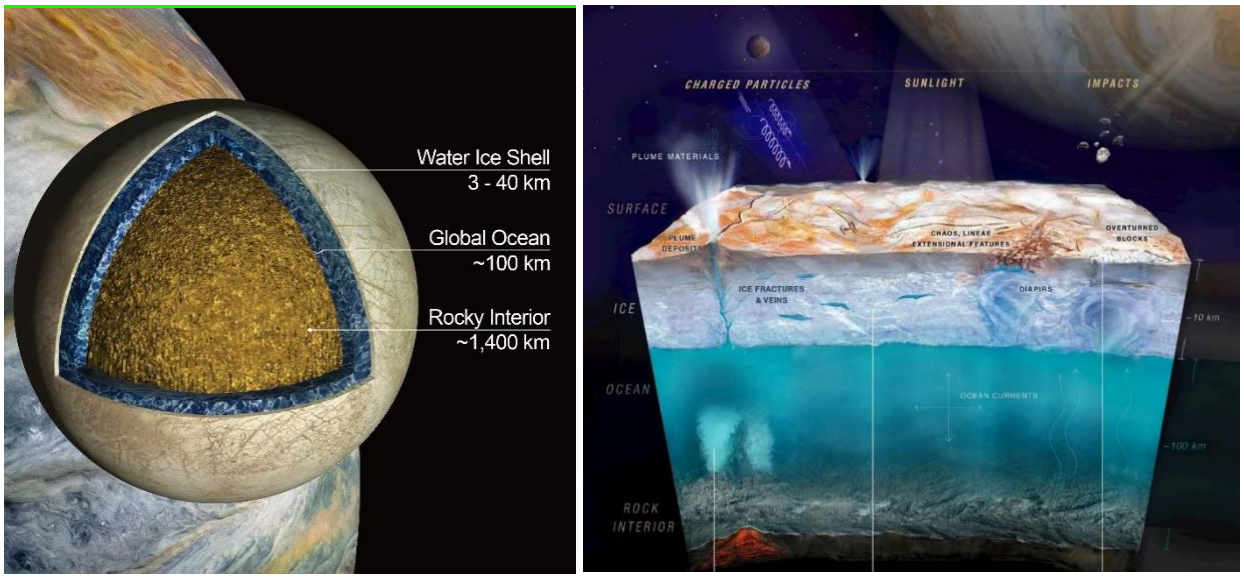

Figure 1: (Left) schematic showing the interior structure of Europa (from Howell & Pappalardo, 2020), (right) a cross-sectional view of Europa's ocean and ice shell (from Hand et al., 2017)

Europa's liquid water is the result of the gravitational interactions between Europa, Jupiter, Ganymede, and Io. The orbit of Europa is in resonance with the orbits of these two

moons, which means that for every two times Europa orbits Jupiter, Io orbits four times and Ganymede orbits once. The resonance causes Europa's orbit to be slightly elliptical instead of circular. The variations of distance to Jupiter and speed of the satellite during an orbit change the amplitude and direction of the tide caused by Jupiter. The heat generated by this process is sufficient to keep Europa's ocean in a liquid state (Cassen et al., 1979). The presence of the global ocean makes Europa a prime location to search for extraterrestrial life, since all life that we know of requires the presence of liquid water.

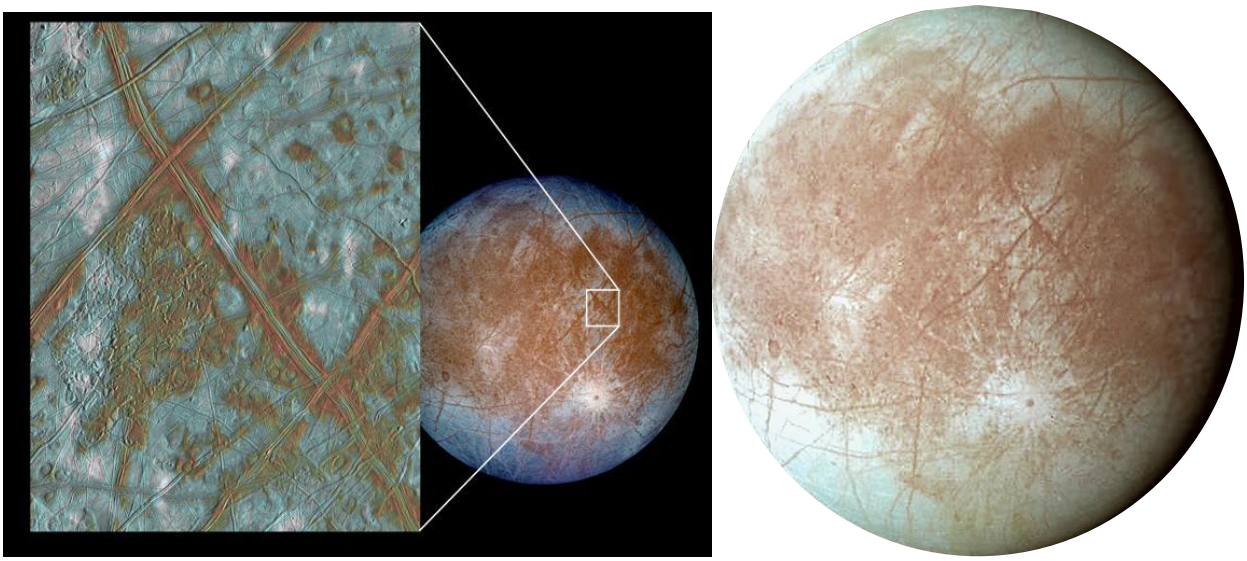

Figure 2: (Left) global view of Europa with close up view of the region near Conamara Chaos, from NASA/JPL Photojournal, (right) global view of Europa showing its many linear tectonic features, from JPL

Studying Europa's surface features and the processes that may form them is an important aspect of understanding the potential habitability of the moon. As seen in Figure 2, global-scale linear features, called lineae, cover the surface of the ice shell. One type of lineae have positive relief and are called ridges. They are the focus of this study. There are multiple types of ridges, and two types focused on here are double ridges and ridge complexes (Head et al., 1999). Double ridges are defined by two topographically high ridge crests and a topographically low central trough (Figures 3.2 and 4). Ridge complexes, also referred to as complex ridges, are composed of multiple ridge crests and troughs (Figure 3.3). These can sometimes appear straight or as overlapping double ridges with sinuous margins. Head et al. (1999) documented a spectrum of ridge morphologies ranging from isolated troughs to double ridges to ridge complexes (Figure 3). They proposed that ridges transition from one morphology to another and increase in complexity as they experience more strain. Examples of double ridges transitioning into ridge complexes suggest a common origin for all types of ridges (Johnston & Montési, 2014).

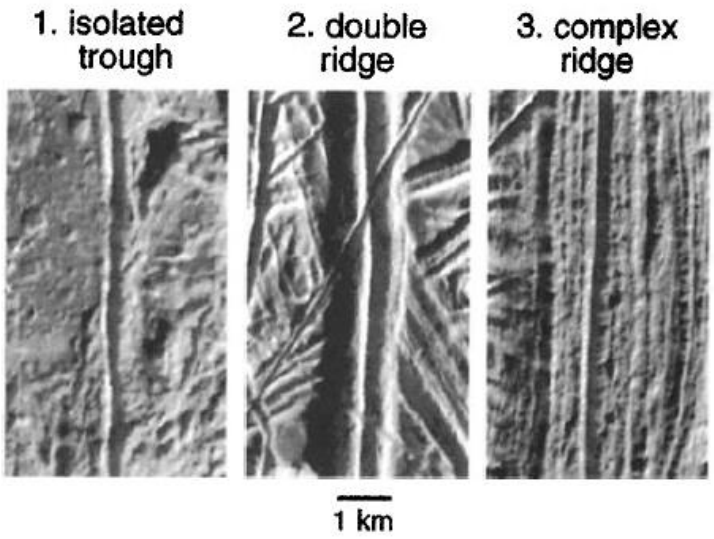

Figure 1: Categories of ridge morphologies, adapted from Head et al. (1999)

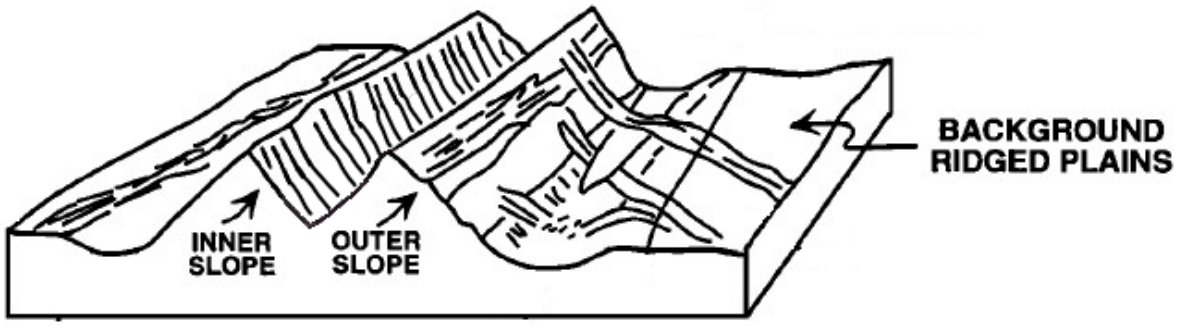

Figure 2: Cross-sectional view of a double ridge showing the two characteristic topographic highs and central trough, as well as the observation that background features can be traced on the flanks of the ridges (adapted from Head et al., 1999)

Multiple explanations have been proposed to explain the formation of double ridges. However, little work has been done to explain ridge complexes. One hypothesis for the formation of double ridges, proposed by Nimmo and Gaidos (2002), is that they are the result of heating caused by strike-slip motion on a vertical fault (Figure 5). In that model, the tidal shear stress on diurnal time scales causes localized shear motion. This motion in turn causes the ice to warm and possibly subside as it melts or sublimates, explaining the central topographic low in double ridges. The two topographically high ridge crests may be explained by thermal uplift around the shear zone in this model (Nimmo & Gaidos, 2002).

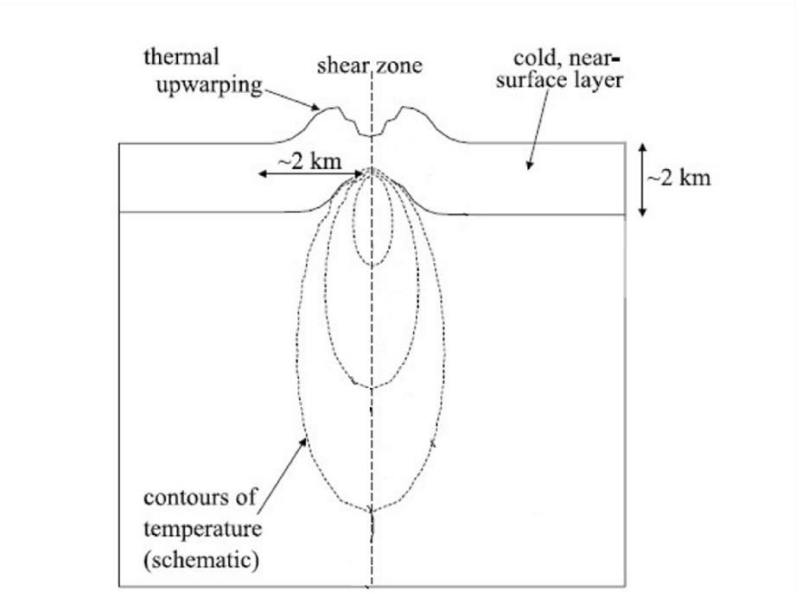

Figure 3: Cross-sectional view of a double ridge showing a proposed formation model involving shear heating, adapted from Nimmo & Gaidos (2002)

Another hypothesis put forward by Melosh and Turtle (2004) is that double ridges could form due to incremental ice-wedging, where material falls into the opening during periods of extension, which prevents the trough from closing completely. Over many tidal cycles, this would form the distinctive double ridge morphology (Melosh & Turtle, 2004). This idea was expanded upon by Johnston and Montési (2014), whose hypothesis indicates that double ridges could be formed due to a crystallizing water intrusion within the ice shell (Figure 6). In this model, a dike-like intrusion forms two high-stress lobes on each side of the intrusion, which raises the ground and produces two elevated crests separated by a central trough (Johnston & Montési, 2014). These models suggest that the transport of water within the ice shell may play an important part in double ridge formation.

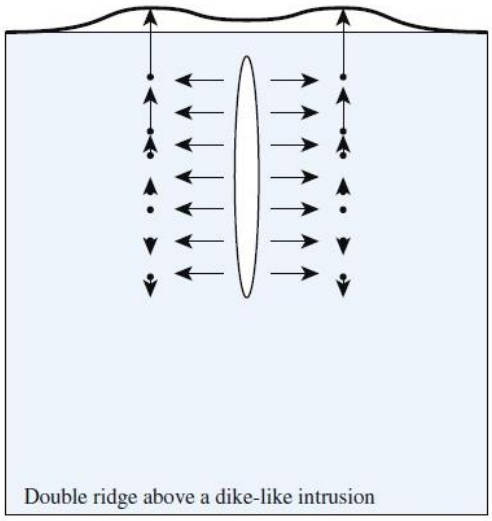

Figure 4: Cross-sectional view showing a proposed formation model using a crystallizing water intrusion to form the double ridge morphology (adapted from Johnston & Montési, 2014)

Objectives of Research and Broader Implications:

We follow the hypothesis, posed by Head et al. (1999), that strain controls the difference between ridge morphologies. They envisioned that the magnitude of strain would be larger in complex ridges than in double ridges, under the view that ridges are dominated by extension. As more recent models have discussed the importance of shear motion in ridge formation (Nimmo & Gaidos, 2002), we also evaluate if the strain regime might be different from one ridge type to another. Quantifying the magnitude and what type of strain controls ridge morphology could influence the understanding of how these features form. Ridges may be good locations for future missions to detect evidence of life, given that they are potential places where material from the subsurface ocean could be transported to the surface.

The potential habitability of icy satellites, especially Europa and Ganymede, is a principal driver of current astrobiology and planetary science research. As such, there are multiple planned missions to the Jovian system. The European Space Agency's JUpiter ICy moons Explorer, or JUICE, is planned to launch in 2023. It will focus mainly on Ganymede, but it will fly by Europa. NASA also has a planned mission to the Jupiter system called Europa Clipper, which is set to launch in 2024, with a predominant focus on Europa. Both missions seek to understand the habitability of icy satellites and the likelihood of finding extraterrestrial life within our solar system. There is also potential for a future lander mission to be sent to Europa (Howell & Pappalardo, 2020). Understanding the type of strain ridges accommodate will expand the understanding of where on Europa to look for evidence of life, which will inform Europa Clipper, JUICE, and other future missions.

Methods:

We mapped a selection of ridges at a scale of 1:400,000 for which each image has a resolution better than 250 m/pixel. The images were examined using *ArcGIS Pro*, which features a multi-resolution mosaic of Galileo Solid-State Imaging (SSI) images prepared by the United States Geological Survey (USGS) Astrogeology Science Center. *ArcGIS Pro* makes it possible to collect the coordinates of vertices that outline ridges of interest, the coordinates of locations where background features are cut by the ridge, as well as the orientation of the background features. The strain across the ridge can be calculated using these offset background features, following the procedure described below. We compared the magnitude of shear strain to normal strain between the different types of ridges in order to test the hypothesis.

Ridges are long, quasi-linear features in map view, with an essentially constant width. Ignoring, for now, complications such as the existence of several subunits in the most complex ridges, each linea can be approximated as a long rectangle with width Y and orientation β, defined as the angle between the margin of the feature and the North direction. The displacement across the ridge is defined as a shear offset dx and opening dy. The initial width of the ridge is assumed to be y_0 (Figure 7), so that the current width is

$$Y = y_0 + dy \quad (1)$$

where y_0 corresponds to the width of the region that is not influenced by strain.

Strain across a ridge is evaluated by considering how a pre-existing background feature is offset by the ridge of interest. We report the coordinates of endpoints of these background features, linked by a tie-line across the studied ridge. Documenting the shear offset and opening

is not as simple as projecting the tie-line in the directions parallel and normal to the feature of interest. A component of the tie-line offset is due to a portion of the background feature now hidden in the resurfaced region. A geometric analysis shows that this offset depends on θ, the angle between the ridge-normal direction (Figure 7) and the linear background feature.

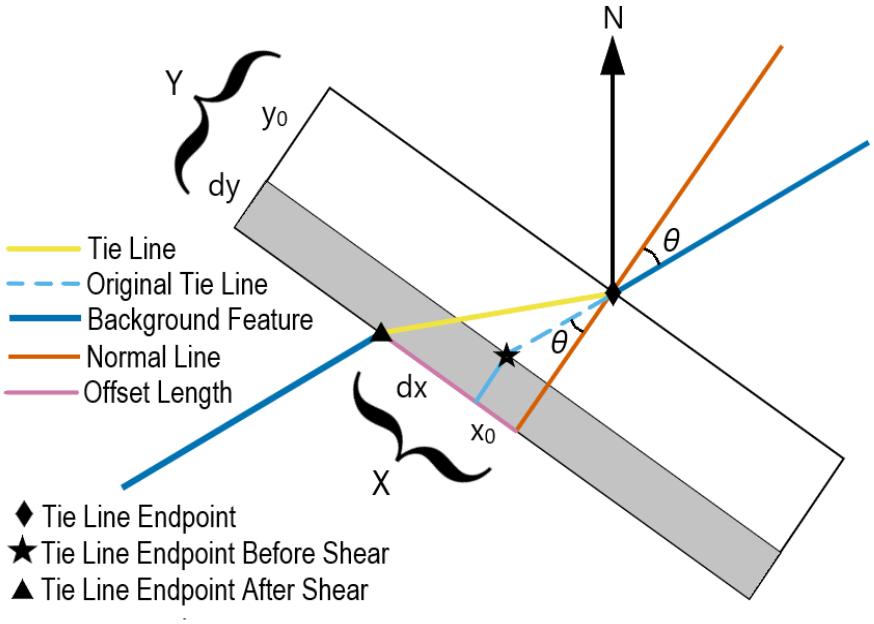

Figure 5: Idealized geometry of a ridge undergoing shear and extension. The region in the white rectangle has been resurfaced without strain, providing an initial width y_0 to the ridge. The ridge interrupts a preexisting linear background feature (blue line). The angle θ is defined between the background feature and the orientation normal to the ridge (orange line). Because of this orientation and the nonzero width of the ridge, the background feature appears offset from one side of the ridge to the other even in the absence of deformation (original tie line shown as a dashed blue line joining the diamond and star symbols). This initial offset length is x_0. The actual offset (pink), X, measured using the present tie line (yellow, joining the diamond and triangle symbols) is the initial offset plus any shear motion, dx. After extension by an amount dy (grey rectangle), the ridge reaches its final width, Y.

Per construction, the length of the line projected in the ridge-normal direction is the width of the ridge, Y. The original background feature has an offset

$$x_0 = y_0 \tan(\theta) \quad (2)$$

from the normal line in the ridge-parallel direction (Figure 7), given that the background feature is not necessarily normal to the ridge of interest. The shear offset dx is added to this original distance to form the currently observed offset of the background feature from the normal line, X:

$$X = dx + y_0 \tan\theta \quad (3)$$

We measured the orientation of selected ridges as well as the orientations of several background features cut by the ridge. If the clockwise angle between the background feature and the north direction is α, then

$$\theta = (\beta + 90°) - \alpha \quad (4)$$

For each background feature, we measured the length of the normal line, Y, and the distance from the normal line to the offset feature, X (Figure 7). We make a scatter plot comparing X and $\tilde{x} = \tan\theta$, as Equation 3 shows that these quantities should be linearly related. Deviations from the linear relation may indicate different episodes of deformation or the presence of different strands in the ridges. If the measurements appear roughly linear, we then

calculate a line of best fit using a least-square fit, $X = dx + y_0\tilde{x}$, where dx is the intercept and y_0 is the slope of the best fit line. The dilation is then calculated as the average of $dy = Y - y_0$. The shear strain (γ) and normal strain (ε) are then defined from the offsets as

$$\gamma = \frac{dx}{y_0} = \frac{X}{y_0} - \tan(\theta) \tag{5}$$

and

$$\varepsilon = \frac{dy}{y_0} = \frac{Y}{y_0} - 1 \tag{6}$$

The external strain regime is reported as

$$R = \frac{\gamma}{\varepsilon} = \frac{dx}{dy} \tag{7}$$

Results:

We mapped ridges in two regions: near Conamara Chaos and near the Tyre multiring structure. In the Conamara region, there were two ridge complexes, Agave Linea and Asterius Linea, and one double ridge, Androgeos Linea. The Tyre region has two double ridges, one in the northeast and one in the southwest. For each ridge, we map the entire margins of the ridge, background features that are crossed by the ridge, local margins of the ridge near each background feature, the width of the ridge normal to the margin, the tie-line connecting the two points where the background feature crosses the ridge, and the offset from the normal line to the tie-line endpoint. These mapped regions are shown in Figures 8 and 9.

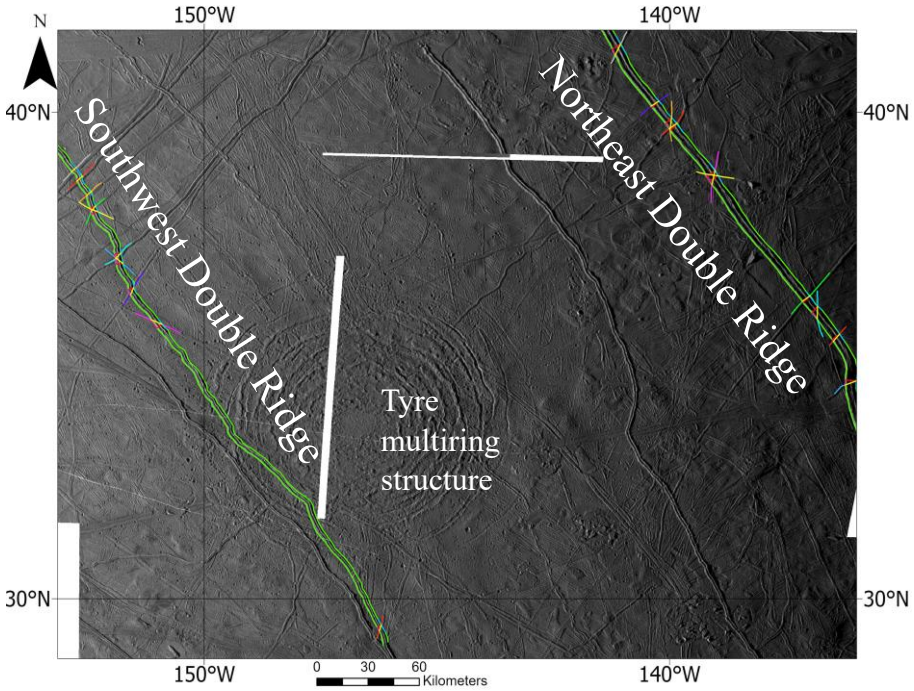

Figure 6: Mapping in the region near the Tyre multiring structure, showing one double ridge in the northeast and another in the southwest

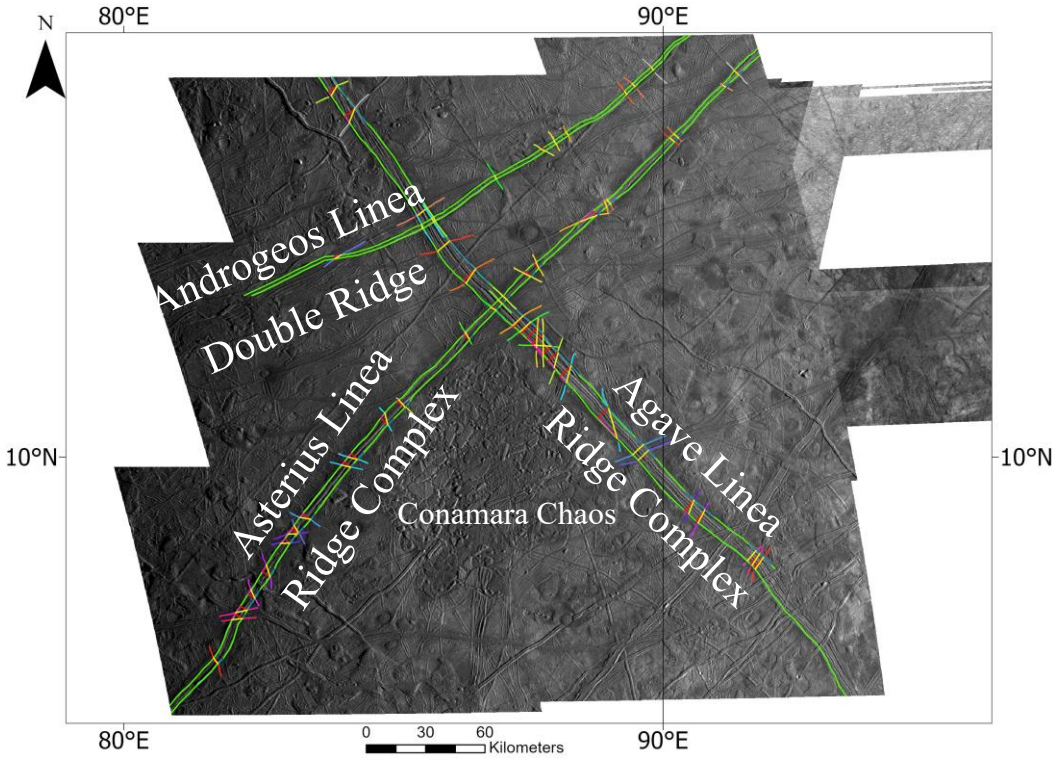

Figure 7: Mapping in the region near Conamara Chaos, showing one double ridge (Androgeos Linea) and two ridge complexes (Asterius Linea and Agave Linea)

Using the measurements of each ridge and the equations given above, we plot the offset width X against $\tilde{x} = \tan\theta$. We then use a linear regression to calculate a best fit line based on Equation 3. The data from all five ridges are shown in Figure 10.

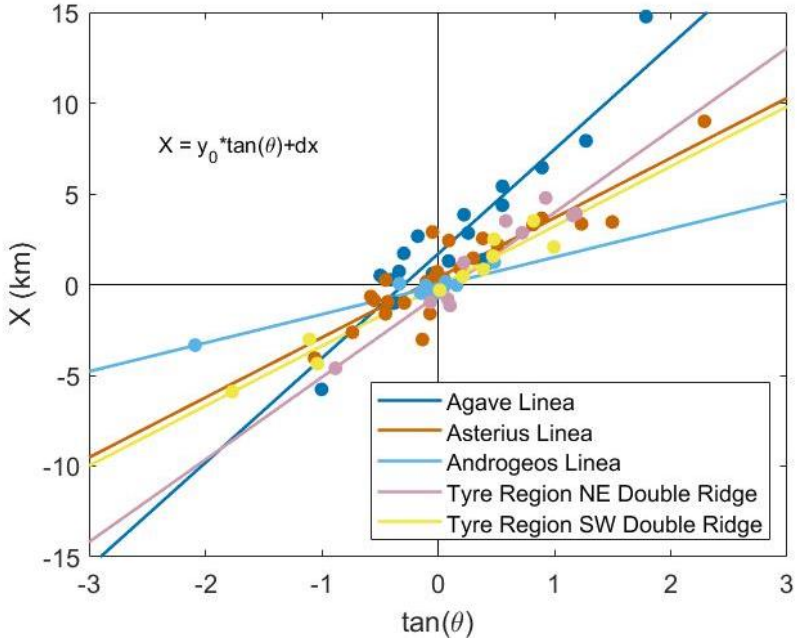

Figure 8: Plot showing the offset width X and $tan\,\theta$ with best fit lines based on Equation 3 for each ridge

From the best fit line and Equation 3, the slope is equal to the initial width y_0, and the intercept is equal to the offset distance dx. We also calculate the average width Y_{av} for each ridge based on the individual widths at each background feature and the extensional width dy (Table 1). The standard deviation ($\sigma_{Y_{av}}$) associated with the average width (Y_{av}) is reported. The uncertainties associated with the initial width (σ_{y_0}) and the offset distance (σ_{dx}) were generated by the linear fit. The uncertainty associated with the extensional width (σ_{dy}) was calculated using the following equation:

$$\sigma_{dy} = dy\sqrt{\left(\sigma_{Y_{av}}\right)^2 + \left(\sigma_{y_0}\right)^2} \tag{8}$$

Using these and Equations 5 and 6, we calculate the normal strain ε and shear strain γ. The uncertainties associated with normal strain (σ_ε) and shear strain (σ_γ) are calculated using the following equations:

$$\sigma_\varepsilon = \varepsilon\sqrt{\left(\frac{\sigma_{dy}}{dy}\right)^2 + \left(\frac{\sigma_{Y_{av}}}{Y_{av}}\right)^2} \tag{9}$$

and

$$\sigma_\gamma = \gamma\sqrt{\left(\frac{\sigma_{dx}}{dx}\right)^2 + \left(\frac{\sigma_{y_0}}{y_0}\right)^2} \tag{10}$$

Table 1: Measurements of initial width (y_0), offset distance (dx), average width (Y_{av}), extensional width (dy), normal strain (ε), shear strain (γ), and all associated uncertainties. Negative values in shear offset and shear strain imply right-lateral strike-slip motion. RC means ridge complex, and DR means double ridge. All distances are expressed in kilometers.

Linea	$\boldsymbol{y_0}$	$\boldsymbol{dx}$	$\boldsymbol{Y_{av}}$	$\boldsymbol{dy}$	$\boldsymbol{\varepsilon}$	$\boldsymbol{\gamma}$
Agave (RC)	5.8 ± 1.2	1.7 ± 0.77	7.1 ± 0.54	1.4 ± 1.8	0.19 ± 0.25	0.29 ± 0.15
Asterius (RC)	3.3 ± 0.66	0.38 ± 0.49	3.7 ± 0.85	0.36 ± 0.39	0.1 ± 0.11	0.11 ± 0.15
Androgeos (DR)	1.6 ± 0.39	-0.07 ± 0.26	1.9 ± 0.19	0.37 ± 0.16	0.19 ± 0.09	-0.04 ± 0.16
Tyre NE (DR)	4.5 ± 1.1	-0.57 ± 0.82	5.6 ±0.53	1.1 ± 1.4	0.2 ± 0.24	-0.13 ± 0.18
Tyre SW (DR)	3.3 ± 0.63	-0.09 ± 0.55	3.6 ± 0.44	0.27 ± 0.21	0.08 ± 0.06	-0.03 ± 0.17

From the data given in Table 1, we compare both the shear (γ) and normal (ε) strains to the average width for each ridge (Y_{av}) (Figure 11). For normal strain, extension plots as a positive value, and contraction plots as a negative value. For shear strain, positive indicates left-lateral strike-slip motion, and negative indicates right-lateral motion. When we account for uncertainties, we do see some extension. The uncertainties for our shear strain are not significantly different from zero strain, so there are no conclusive patterns we can draw from this limited data.

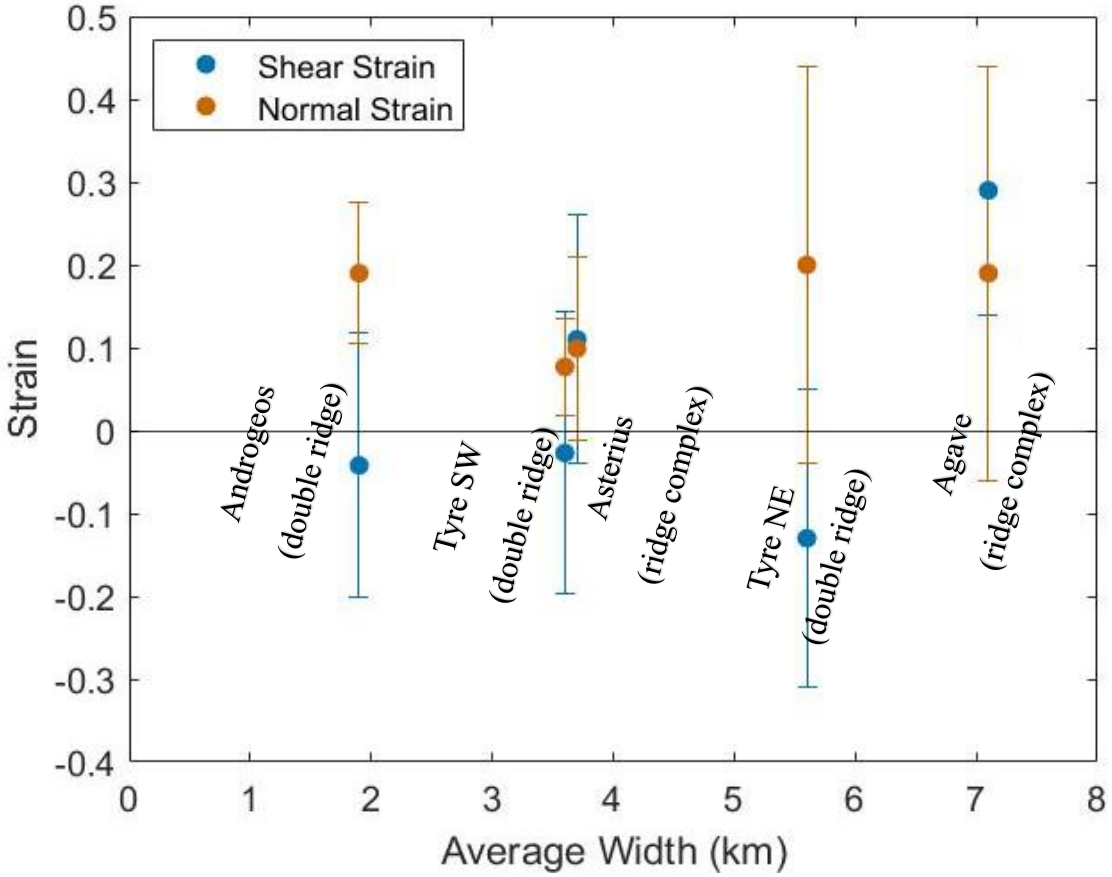

Figure 9: Plot showing both normal strain (orange) and shear strain (blue) as a function of average ridge width. Positive normal strain indicates extension, and negative indicates contraction. Positive shear strain indicates left-lateral motion, and negative indicates right-lateral motion.

The measured widths Y of each ridge do not differ significantly from their initial width y_0 when accounting for their associated uncertainties (Table 1). Therefore, no significant normal strain appears associated with the formation of these ridges. Shear strain cannot be resolved either (Figure 11). This lack of evidence for differential motion of the preexisting surface between the two sides of any linea implies that the main process involved in the formation of both double ridges and ridge complexes is overprinting, with no more than 20% extension.

Discussion:

Two relevant works which used similar observations have been completed by Culha et al. (2014) and Coulter (2009). Though their methods were slightly different, they analyzed some of the same ridges that we have, allowing me to make a direct comparison between my work and theirs. The only ridge that cannot be compared is Asterius Linea, but the other four ridges were analyzed by either Culha et al. (2014) or Coulter (2009) or both.

Culha et al. (2014) follow a very similar methodology to my work. They measure offsets of background features associated with both dilation and shear. They analyze the geometry using a similar method to mine, which accounts for the total offset and incidence angle of the background feature. Like my work, they plot their data, calculate a best fit line, and interpret the

intercept of the line as the strike-slip offset. Our methods differ because they interpret the slope of the line as the expansion, where we interpret this as the initial width. In their interpretation, the initial width, y_0, the total width, Y_{av}, and the extensional width, dy, are all the same value. My work has shown that there is indeed an initial width for ridges, so assuming that the entire width is the product of extension is not an accurate assumption. Included in the ridges they mapped were Agave Linea, Androgeos Linea, and the southwest double ridge in the Tyre region.

Coulter (2009) begins with similar observations of background features, the associated incidence angle, and their offsets due to dilation and shear. Their methods differ here because they define a separation based on the total width of the ridge and the offset between the endpoints of background features. This allows them to plot the separation against the incidence angle. They plot theoretical curves of what would be expected from pure extension, pure right-lateral motion, pure left-lateral motion, and comparative ratios between shear and dilation. They then compare the data from each ridge to find which strain regime most closely matches their data. They report the ratio of strike-slip to dilation. Among the ridges they mapped were Agave Linea, Androgeos Linea, and the northeast double ridge in the Tyre region.

My results from Agave Linea, the ridge complex in the Conamara region, can be compared to both Culha et al. (2014) and Coulter (2009). We found an extensional width of 1.4 ± 1.8 km, with an initial width of 5.8 ± 1.2 km, and a left-lateral strike-slip offset of 1.7 ± 0.77 km. Culha et al. (2014) found 2.19 ± 0.37 km of extension, and a strike slip offset of -1.99 ± 0.13 km (the negative implies left-lateral motion). Coulter (2009) reported 970 m (0.970 km) of extension in the northern part and 452 m (0.452 km) of extension in the southern part. They also find ~3.1 km of left-lateral strike-slip offset in the northern part and ~2.3 km of left-lateral strike-slip offset in the southern part. This results in a -3.2:1 ratio of left-lateral shear to dilation in the northern part and -4.6:1 in the southern part. Both the results from Coulter (2009) and Culha et al. (2014) for the extensional width fall within my uncertainties. The magnitudes of the shear offsets from Culha et al. (2014) and the northern part of Agave Linea from Coulter (2009) fall within my uncertainties. However, the southern part of Agave Linea from Coulter (2009) is larger than the values from both Culha (2014) and I, though we all find evidence of left-lateral motion.

Androgeos Linea is the double ridge in the Conamara region. We find an extensional length of 0.37 ± 0.16 km, an initial width of 1.6 ± 0.39 km, and a right-lateral strike-slip offset of -0.07 ± 0.26 km. Coulter (2009) found an extensional width of 56 m (0.056 km) and a 10:1 right-lateral strike-slip to dilation ratio (they don't report the strike-slip offset in m). Culha et al. (2014) found 0.30 ± 0.03 km of extension and 0.14 ± 0.03 km of right lateral strike slip motion. My values are in agreement with those from Culha et al. (2014) for both extension and shear offset. The value for extension from Coulter (2009) is much smaller than the value from both Culha et al. (2014) and I, though all three report right-lateral strike-slip motion.

In the Tyre region, there are two double ridges. For the double ridge in the northeast, er found 1.1 ± 1.4 km of extension, with an initial width of 4.5 ± 1.1 km, and a right-lateral strike-slip offset of -0.57 ± 0.82 km. Coulter (2009) also analyzed this ridge, and found an extensional width of 305 m (0.305 km), and a right-lateral strike-slip offset of 1189 m (1.189 km). This gave a strike-slip to dilation ratio of 3.9:1. Both the values for shear offset and extension found by Coulter (2009) fall within the range of my uncertainties. For the southwest double ridge in the Tyre region, we found 0.27 ± 0.21 km of extension, with an initial width of 3.3 ± 0.63 km, and a

right-lateral strike-slip offset of -0.09 ± 0.55 km. Culha et al. (2014) found -0.28 ± 0.18 km of dilation, meaning they found evidence for contraction. They also report -0.09 ± 0.11 km left-lateral offset. While the values for shear offset are consistent withing the uncertainties, dilations are different with Culha et al. (2014) finding contraction while we found extension.

The majority of the data we have collected matches well with the results from both Coulter (2009) and Culha et al. (2014). The main contrast between their assumptions and mine were my inclusion of an initial width for the features we observe, though they both do discuss that any results for their extensional values do not explain the entire width for the features. Culha et al. (2014) reports global surface strain for double ridges as 2.22 ± 0.76 % contraction, while we did not find evidence for contraction associated with any of the ridges we analyzed.

Overall, the data seem to show variable amounts of dilation and shear motion. There does not seem to be a correlation between the type of strain and the type of ridge. There does appear to be a non-zero amount of extension associated with the formation of ridges, but this extension does not explain the entire widths of the ridges. Therefore, there is a non-zero initial width associated with the formation of ridges. Since there is some initial width in the formation of ridges, the features that we see must form at least partially in place, without the involvement of either shear or normal strain. The formation mechanism for ridges on Europa must involve overprinting, where the ice deforms in place. This is unlike the results reported from Culha et al. (2014) and Coulter (2009), because they make the assumption that ridges form from a crack with no initial width. My results are supported by the observation of background features sometimes appearing on the flanks of double ridges (Head et al., 1999).

Since my analysis does not rely on the assumption that ridges must form from an initial crack like Culha et al. (2014) and Coulter (2009), my results may be applied to a broader range of formation mechanisms. This analysis has implications for the formation mechanisms that may be associated with ridges. Localized uplift produced by cryovolcanism would explain the topography of the ridge crests observed in both double ridges and ridge complexes, and might not involve much normal or shear strain, which fits with the observations from this work. A subsurface cryomagma intrusion, like a dike or warm diapir, could also explain the lack of strain and be a viable formation mechanism. The association with such formation mechanisms could mean that ridges may be locations associated with subsurface water transport. The transport of water within Europa's ice shell means that a suitable environment for the development of life may exist near the surface of the ice shell, or that essential nutrient transport between the surface of the ice shell and the subsurface ocean may exist. Therefore, ridges may be a location to be targeted by future missions, like Europa Clipper, to look for evidence of life.

Conclusions:

My work has demonstrated that a geometric analysis of surface features on Europa can determine the shear and normal strains associated with ridge formation. This method functions with fewer assumptions of formation mechanism than previous studies. We find small amounts of shear and normal strains associated with the formations of both double ridges and ridge complexes, with slightly more normal strain than shear strain. However, these strains do not explain the entire width of the feature observed, so some portion of ridge formation must be controlled by overprinting, or deformation in place. This observation of an initial width involved in ridge formation is consistent with proposed formation models involving water transport within Europa's ice shell, such as a cryovolcanic intrusion, like a dike or warm diapir. This potential

association with water transport could mean that ridges may contain evidence of life if it exists on Europa, which can help inform future missions such as Europa Clipper.

Bibliography:

Anderson, J.D., Schubert, G., Jacobson, R.A., Lau, E.L., Moore, W.B., Sjogren, W.L., 1998. Europa's Differentiated Internal Structure: Inferences from Four Galileo Encounters. Science 281, 2019-2022. https://doi.org/10.1126/science.281.5385.2019

Cassen, P., Reynolds, R.T., Peale, S.J., 1979. Is there liquid water on Europa?. J. Geophys. Res. Lett. 6, 731-734. https://doi.org/10.1029/GL006i009p00731

Coulter, 2009. Kinematic and morphological evolution of Europa's ridges (unpublished master's thesis). University of Idaho.

Culha, C., Hayes, A.G., Manga, M., & Thomas, A.M., 2014. Double ridges on Europa accommodate some of the missing surface contraction. J. Geophys. Res. Planets 119, 395-403. https://doi.org/10.1002/2013JE004526

Figueredo, P.H., Greeley, R., 2000. Geologic mapping of the northern leading hemisphere of Europa from Galileo solid-state imaging data. J. Geophys. Res. 105, 22629-22646. https://doi.org/10.1029/1999JE001107

Figueredo, P.H., Greeley, R., 2004. Resurfacing history of Europa from pole-to-pole geological mapping. Icarus 167, 287-312. https://doi.org/10.1016/j.icarus.2003.09.016

Hand, K.P., Murray, A.E., Garvin, J.B., Brinckerhoff, W.B., Christner, B.C., Edgett, K.S., Ehlmann, B.L., German, C.R., Hayes, A.G., Hoehler, T.M., Horst, S.M., Lunine, J.I., Nealson, K.H., Paranicas, C., Schmidt, B.E., Smith, D.E., Rhoden, A.R., Russel, M.J., Templeton, A.S., Willis, P.A., Yingst, R.A., Phillips, C.B., Cable, M.L., Craft, K.L., Hofmann, A.E., Nordheim, T.A., Pappalardo, R.P., and the Project Engineering Team (2017): Report of the Europa Lander Science Definition Team. Posted February, 2017

Head, J., Pappalardo, R, Sullivan, R., 1999. Europa: Morphological characteristics of ridges and triple bands from Galileo data (E4 and E6) and assessment of linear diapirism model. J. Geophys. Res. Planets 104, 24223-24236. https://doi.org/10.1029/1998JE001011

Howell, S.M., Pappalardo, R.T., 2018. Band Formation and Ocean-Surface Interaction on Europa and Ganymede. Geophys. Res. Lett. 45, 4701-4709. https://doi.org/10.1029/2018GL077594

Howell, S.M., Pappalardo, R.T., 2020. NASA's Europa Clipper — a mission to a potentially habitable world. Nat. Commun. 11, 1311. https://doi.org/10.1038/s41467-020-15160-9

Johnston, S., Montési, L., 2014. Formation of ridges on Europa above crystallizing water bodies inside the ice shell. Icarus 237, 190-201. https://doi.org/10.1016/j.icarus.2014.04.026

Kattenhorn, S.A., Hurford, T.A., 2009. Tectonics of Europa. In R.T. Pappalardo, W.B. McKinnon, & K. Khurana (Eds.), *Europa* (pp. 199-236). Tucson: University of Arizona Press.

Kattenhorn, S.A., Prockter, L.M., 2014. Evidence for subduction in the ice shell of Europa. Nat. Geosci. 7, 762-767. https://doi.org/10.1038/ngeo2245

Khurana, K.K., Kivelson, M.G., Stevenson, D.J., Schubert, G., Russell, C.T., Walker, R.J., Polanskey, C., 1998. Induced magnetic fields as evidence for subsurface oceans in Europa and Callisto. Nature 395, 777-780. https://doi.org/10.1038/27394

Melosh, H.J., Turtle, E.P., 2004. Ridges on Europa: Origin by Incremental Ice-Wedging. Lunar Planet. Sci. XXXV. Abstract #2029

Nimmo, F., Gaidos, E., 2002. Strike-slip motion and double ridge formation on Europa. J. Geophys. Res. Planets 107, 5-1-5-8. https://doi.org/10.1029/2000JE001476

Prockter, L.M., Head, J.W., Pappalardo, R.T., Sullivan, R.J., Clifton, A.E., Giese, B., Wagner, R., Nuekum, G., 2002. Morphology of Europan bands at high resolution: A mid-ocean ridge-type mechanism. J. Geophys. Res. Planets 107, 4-1-4-26. https://doi.org/10.1029/2000JE001458

Roth, L., Saur, J., Retherford, K., Strobel, D., Feldman, P., McGrath, M., Nimmo, F., 2014. Transient Water Vapor at Europa's South Pole. Science 343, 171-174. https://doi.org/10.1126/science.1247051